ROBUST AND RELIABLE DNS AND LES ON UNSTRUCTURED GRIDS

***F. X. Trias*[1], *J. A. Hopman*[1], *D. Santos*[1], *A. Gorobets*[2] *and A. Oliva*[1]**

[1] ***Heat and Mass Transfer Technological Center,***
Technical University of Catalonia, C/Colom 11, 08222 Terrassa (Barcelona), Spain.
[2] ***Keldysh Institute of Applied Mathematics, 4A, Miusskaya Sq., Moscow 125047, Russia***
francesc.xavier.trias@upc.edu

Abstract

Preserving the operators symmetries at discrete level is the key aspect to enable reliable DNS and LES simulations of turbulent flows. On the other hand, real-world applications demand robust and stable numerical methods suitable for complex geometries. In this regard, this work presents a symmetry-preserving discretization for unstructured collocated grids that, apart from being virtually free of artificial dissipation, it is shown to be unconditionally stable. Special attention is given to the (de)construction of the discrete operators into fundamental geometrical entities. On this basis, a new inexpensive method to compute strict eigenbounds for the convective and diffusive operators, which are needed to determine the time-step *à la* CFL, is presented. Apart from providing better estimations than previous methods, it is relies on a sparse-matrix vector product where only vectors change on time. Hence, both implementation in existing codes and cross-platform portability are straightforward. Altogether leads to a simple and robust approach for DNS and LES simulations of complex turbulent flows.

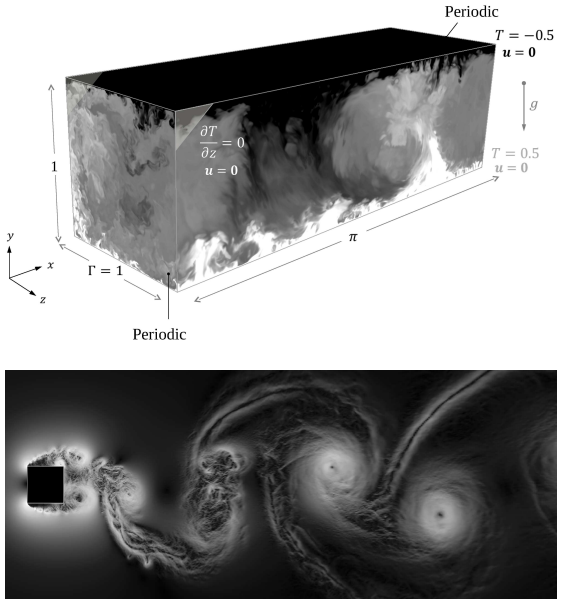

Figure 1: Examples of DNSs computed using symmetry-preserving discretizations. Top: Rayleigh–Bénard configuration studied in Dabbagh et al. (2020). Bottom: turbulent flow around a square cylinder at $Re = 22000$ studied in Trias et al. (2015).

1 Introduction

The essence of turbulence are the smallest scales of motion. They result from a subtle balance between convective transport and diffusive dissipation. Mathematically, these terms are governed by two differential operators differing in symmetry: the convective operator is skew-symmetric, whereas the diffusive is symmetric and negative-definite. At discrete level, operator symmetries must be retained to preserve the analogous (invariant) properties of the continuous equations (see Verstappen and Veldman (2003); Trias et al. (2014)): namely, the convective operator is represented by a skew-symmetric matrix, the diffusive operator by a symmetric, negative-definite matrix and the divergence is minus the transpose of the gradient operator. It is noteworthy to mention that in the last decade, many DNS reference results have been successfully generated using this type of discretization (see Figure 1, for example). Moreover, we also consider that symmetry-preserving discretizations form a solid basis for testing sub-grid scale models for LES. Namely, for coarse grids, the energy of the resolved scales of motion is convected in a stable manner, *i.e.* the discrete convective operator transports energy from a resolved scale of motion to other resolved scales without dissipating any energy, as it should be from a physical point-of-view.

2 Symmetry-preserving discretization on unstructured grids

For unstructured meshes, it is (still) a common argument that local accuracy should take precedence over the properties of the operators. Contrary to this, our philosophy is that operator symmetries are critical to the dynamics of turbulence and must be preserved. With this in mind, a fully-conservative discretization method for general unstructured grids was proposed in Trias et al. (2014): it exactly preserves the symmetries of the underlying differential operators on a collocated mesh. In summary, and following the same

notation, the method is based on a set of five basic operators: the cell-centered and staggered control volumes (diagonal matrices), Ω_c and Ω_s, the matrix containing the face normal vectors, N_s, the cell-to-face scalar field interpolation, $\Pi_{c\to s}$ and the cell-to-face divergence operator, M. Once these operators are constructed, the rest follows straightforwardly from them. Hence, as shown in Komen et al. (2021), the proposed method constitutes a robust and easy-to-implement approach to solve incompressible turbulent flows in complex configurations that can be easily implemented in already existing codes such as OpenFOAM®.

3 Pressure-velocity coupling: reconciling accuracy and robustness

Pressure-correction methods on collocated grids suffer two inherent drawbacks: the cell-centered velocity field is not exactly incompressible and some artificial dissipation is inevitably introduced (see Felten and Lund (2006); Trias et al. (2014)). The former error can have severe implications for DNS and LES simulations of turbulent flows since this artificial dissipation can significantly affect the dynamics of the small scales, even overwhelming the dissipation introduced by the subgrid-scale LES models. This was clearly observed in Komen et al. (2017) for LES simulations using OpenFOAM®. It is worth to notice that the ideal target, *i.e.* no artificial dissipation and no checkerboard, can be achieved by explicitly removing those nonphysical components of the pressure field that belong to the kernel of the so-called wide-stencil Laplacian. Alternatively, it is possible to minimize the amount of dissipation while still keeping the solution virtually free of checkerboard modes by preserving the symmetries of the discrete operators (see companion paper by Hopman et al. (2023)). Special attention must be paid to the construction of the face-to-cell and cell-to-face interpolations, in order to guarantee that the numerical method is unconditionally stable (see companion paper by Santos et al. (2023)).

4 A robust and efficient time-integration

Deconstructing convection and diffusion matrices

Let us consider the convective operator

$$\mathsf{C}_c\left(\boldsymbol{u}_s\right) \equiv \mathsf{M}\mathsf{U}_s\Pi_{c\to s} \in \mathbb{R}^{n\times n}, \tag{1}$$

where $\mathsf{M} \in \mathbb{R}^{n\times m}$ is the face-to-cell divergence operator, $\Pi_{c\to s} \in \mathbb{R}^{m\times n}$ is cell-to-face interpolation and $\mathsf{U}_s = \mathrm{diag}(\boldsymbol{u}_s) \in \mathbb{R}^{m\times m}$ is a diagonal matrix that contains the face velocities, $\boldsymbol{u}_s \in \mathbb{R}^m$, that change every time-step. Here, n and m correspond to the total number of mesh cells and faces, respectively. Moreover, the diffusive operator with non-constant (in time) diffusivity reads

$$\mathsf{D}_c(\boldsymbol{\alpha}_s) \equiv \mathsf{M}\Lambda_s\mathsf{G} \in \mathbb{R}^{n\times n}, \tag{2}$$

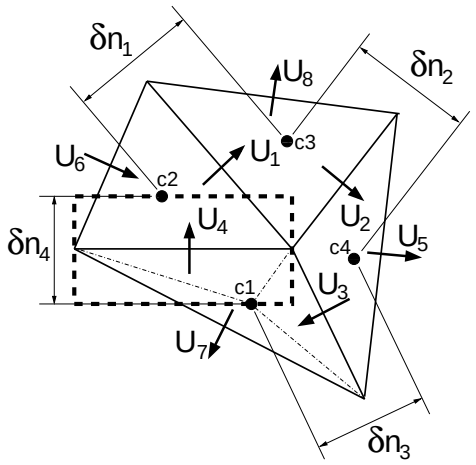

Figure 2: Definition of the volumes, Ω_s, associated with the the face-normal velocities, $\boldsymbol{u}_s$. Thick dashed rectangle is the volume associated with the staggered velocity $\mathrm{U}_4 = [\boldsymbol{u}_s]_4$, *i.e.* $[\Omega_s]_{4,4} = A_4\delta_4$ where A_4 is the face area and $\delta_4 = |\boldsymbol{n}_4 \cdot \overrightarrow{c1c2}|$ is the projected distance between adjacent cell centers.

where $\Lambda_s = \mathrm{diag}(\boldsymbol{\alpha}_s) \in \mathbb{R}^{m\times m}$ is a diagonal matrix containing the diffusivity values at the faces, $\boldsymbol{\alpha}_s \in \mathbb{R}^m$. Notice that this is also relevant for eddy-viscosity turbulence models. For details about the discretization, the reader is referred to the original paper by Trias et al. (2014).

At this point, we aim to answer the following research question: *can we avoid to explicitly reconstruct at each time-step both convective, $\mathsf{C}_c\left(\boldsymbol{u}_s\right)$, and diffusive, $\mathsf{D}_c(\boldsymbol{\alpha}_s)$, matrices while still being able to compute proper eigenbounds in an inexpensive manner?* To do so, let us firstly write the divergence operator, M, in terms of the cell-to-face, $\mathsf{T}_{cs} \in \mathbb{R}^{m\times n}$ and face-to-cell, $\mathsf{T}_{sc} \in \mathbb{R}^{n\times m}$, incidence matrices

$$\mathsf{M} \equiv \mathsf{T}_{sc}\mathsf{A}_s \in \mathbb{R}^{n\times m}, \tag{3}$$

where $\mathsf{A}_s \in \mathbb{R}^{m\times m}$ is a diagonal matrix containing the face surfaces. Moreover, recalling the duality between the divergence and the gradient operators

$$\mathsf{M} = -(\Omega_s\mathsf{G})^T \quad \Longrightarrow \quad \mathsf{G} = -\Omega_s^{-1}\mathsf{M}^T, \tag{4}$$

together with the relation $\mathsf{T}_{sc} = \mathsf{T}_{cs}^T$ leads to

$$\mathsf{G} \equiv -\Omega_s^{-1}\mathsf{A}_s\mathsf{T}_{sc}^T = -\Delta_s^{-1}\mathsf{T}_{cs}, \tag{5}$$

where $\Delta_s \equiv \Omega_s\mathsf{A}_s^{-1} \in \mathbb{R}^{m\times m}$ is a diagonal matrix containing the projected distances, $\delta n_f = |\boldsymbol{n}_f \cdot \overrightarrow{c1c2}|$, between the cell centers, $c1$ and $c2$, of the two cells adjacent to a face, f_4 (see Figure 2). Plugging all this into the definition of the diffusive operator (2) leads to

$$\mathsf{D}_c(\boldsymbol{\alpha}_s) = -\mathsf{T}_{sc}\mathsf{A}_s\Lambda_s\Delta_s^{-1}\mathsf{T}_{cs} = -\mathsf{T}_{cs}^T\tilde{\Lambda}_s\mathsf{T}_{cs}, \tag{6}$$

where the diagonal matrix $\tilde{\Lambda}_s = \mathsf{A}_s\Lambda_s\Delta_s^{-1} \in \mathbb{R}^{m\times m}$ has strictly positive diagonal coefficients. Hence, the

diffusive operator is symmetric and negative semi-definite likewise the continuous Laplacian, ∇^2.

Similarly, the convective term given in Eq.(1) can be written as follows

$$\mathsf{C}_c\left(\boldsymbol{u}_s\right) = \mathsf{T}_{sc}\mathsf{U}_s\mathsf{A}_s\Pi_{c\to s}, \tag{7}$$

where the cell-to-face interpolation, $\Pi_{c\to s}$, defines the numerical scheme we are using. For instance, taking

$$\Pi^{\mathrm{SP}}_{c\to s} = \frac{1}{2}|\mathsf{T}_{cs}| \qquad \text{(mid-point)}, \tag{8}$$

leads to a skew-symmetric matrix, *i.e.* $\mathsf{C}_c\left(\boldsymbol{u}_s\right) = -\mathsf{C}_c^T\left(\boldsymbol{u}_s\right)$ that corresponds to a second-order symmetry-preserving discretization (see Verstappen and Veldman (2003); Trias et al. (2014)). Here $|\mathsf{A}|$ denotes the entry-wise absolute value of a real-valued matrix, *i.e.* $[|\mathsf{A}|]_{ij} = |[\mathsf{A}]_{ij}|$. In summary, convective and diffusive operators read

$$\mathsf{D}_c(\boldsymbol{\alpha}_s) = -\mathsf{T}_{cs}^T\tilde{\Lambda}_s\ \mathsf{T}_{cs}\ , \tag{9}$$

$$2\mathsf{C}_c\left(\boldsymbol{u}_s\right) = \quad \mathsf{T}_{cs}^T\mathsf{F}_s|\mathsf{T}_{cs}|, \tag{10}$$

where $\tilde{\Lambda}_s$ is a diagonal matrix with $[\mathrm{diag}(\tilde{\Lambda}_s)]_i > 0\ \ \forall i$ and $\mathsf{F}_s \equiv \mathsf{A}_s\mathsf{U}_s$ and $\mathrm{diag}(\mathsf{F}_s) \in ker(\mathsf{T}_{cs}^T)$. Notice that, in general, both diagonal matrices $\tilde{\Lambda}_s$ (diffusive fluxes) and F_s (mass fluxes) change on time. Notice that $\mathrm{diag}(\mathsf{F}_s) \in ker(\mathsf{T}_{cs}^T)$ follows from the incompressibility constraint, $\mathsf{M}\boldsymbol{u}_s = \mathbf{0}_c$, and the definition of the divergence operator given in Eq.(3).

Eigenbounds for the diffusion matrix

The idea at this point is to construct other matrices with the same spectrum (except for the zero-valued eigenvalues). To do so, we will use the following well-known property:

Theorem 1. *Let $\mathsf{A} \in \mathbb{R}^{n\times m}$ and $\mathsf{B} \in \mathbb{R}^{m\times n}$ be two rectangular matrices and $m \geq n$. Then, the square matrices $\mathsf{AB} \in \mathbb{R}^{n\times n}$ and $\mathsf{A}^T\mathsf{B}^T \in \mathbb{R}^{m\times m}$ have the same eigenvalues except for the zero-valued ones.*

Therefore, a family of α-dependent matrices with the same spectrum (except for the zero-valued eigenvalues) as those given in Eqs.(9) and (10) can be constructed using Theorem 1. Namely, matrix

$$-\tilde{\Lambda}_s^{\alpha}\mathsf{T}_{cs}\ \mathsf{T}_{cs}^T\ \tilde{\Lambda}_s^{1-\alpha} \qquad \text{(diffusive)}, \tag{11}$$

has the same spectrum as $-\mathsf{T}_{cs}^T\tilde{\Lambda}_s\mathsf{T}_{cs}$. Consequently,

$$\rho(\mathsf{D}_c(\boldsymbol{\alpha}_s)) = \rho(\tilde{\Lambda}_s^{\alpha}\mathsf{T}_{cs}\ \mathsf{T}_{cs}^T\ \tilde{\Lambda}_s^{1-\alpha}). \tag{12}$$

regardless of the values of α. Furthermore, matrices

$$|\mathsf{F}_s|^{\alpha}\mathsf{T}_{cs}|\mathsf{T}_{cs}^T||\mathsf{F}_s|^{-\alpha}\mathsf{F}_s \quad \text{(convective)}, \tag{13}$$

$$|\mathsf{F}_s|^{\alpha-1}\mathsf{F}_s\mathsf{T}_{cs}|\mathsf{T}_{cs}^T||\mathsf{F}_s|^{1-\alpha} \quad \text{(convective)}, \tag{14}$$

have the same spectrum as $\mathsf{T}_{cs}^T\mathsf{F}_s|\mathsf{T}_{cs}|$, respectively. Notice that indeterminate forms $1/0$ may eventually occur for $\alpha < 0$ or $\alpha > 1$ in Eqs.(13) and (14) if a mass flux (diagonal terms of F_s) becomes zero. For instance, the following four matrices have the same spectrum (except for the zero-valued eigenvalues)

$$\Big\{-\mathsf{T}_{cs}^T\tilde{\Lambda}_s\mathsf{T}_{cs}, -\mathsf{T}_{cs}\mathsf{T}_{cs}^T\tilde{\Lambda}_s, -\tilde{\Lambda}_s^{1/2}\mathsf{T}_{cs}\mathsf{T}_{cs}^T\tilde{\Lambda}_s^{1/2}, -\tilde{\Lambda}_s\mathsf{T}_{cs}\mathsf{T}_{cs}^T\Big\}, \tag{15}$$

where the last three correspond to values of $\alpha = 0$, $1/2$, and 1 in Eq.(12), respectively. The advantage of the new forms is that only the matrix $-\mathsf{T}_{cs}\mathsf{T}_{cs}^T$ has to be computed (once) and stored. Note that this face-to-face matrix has -2 in the diagonal and ± 1 in the non-zero off-diagonal elements, which correspond to the faces of the two adjacent control volumes. Then, to find an upper bound (in absolute value) of the eigenvalues, we can apply the Gershgorin circle theorem as follows

$$\rho(\mathsf{T}_{cs}\mathsf{T}_{cs}^T\tilde{\Lambda}_s) \leq \max\{|\mathsf{T}_{cs}\mathsf{T}_{cs}^T|\,\mathrm{diag}(\tilde{\Lambda}_s)\}, \tag{16}$$

$$\rho(\tilde{\Lambda}_s\mathsf{T}_{cs}\mathsf{T}_{cs}^T) \leq \max\{\mathrm{diag}(\tilde{\Lambda}_s) \circ |\mathsf{T}_{cs}\mathsf{T}_{cs}^T|\mathbf{1}_s\}, \tag{17}$$

where $\circ$ denotes the Hadamard product (element-wise product) and $\mathbf{1}_s \in \mathbb{R}^m$ is a vector of ones defined at the faces. As stated above, these three forms correspond to values of $\alpha = 0$, $1/2$ and 1 in Eq.(12), respectively.

Remark 1. *In practice, we need estimations of the spectral radius of $\Omega_c^{-1}\mathsf{D}_c(\boldsymbol{\alpha}_s)$ and not $\mathsf{D}_c(\boldsymbol{\alpha}_s)$. This can be easily done by replacing $|\mathsf{T}_{cs}\mathsf{T}_{cs}^T|$ by $|\mathsf{T}_{cs}\Omega_c^{-1}\mathsf{T}_{cs}^T|$ in Eqs.(16) and (17). An equivalent remark can be made for the forthcoming discussion about the convective matrix, $\mathsf{C}_c\left(\boldsymbol{u}_s\right)$.*

Eigenbounds for the convective matrix

The convective term given in Eq.(10) can be treated similarly. However, in this case, the diagonal matrix F_s (mass fluxes across the faces) can take positive and negative values depending on the flow direction. Similarly to Eq.(15), these five matrices have the same spectrum (except the zero-valued eigenvalues)

$$\Big\{\mathsf{T}_{cs}^T\mathsf{F}_s|\mathsf{T}_{cs}|, \mathsf{T}_{cs}|\mathsf{T}_{cs}^T|\mathsf{F}_s, |\mathsf{F}_s|^{1/2}\mathsf{T}_{cs}|\mathsf{T}_{cs}^T||\mathsf{F}_s|^{-1/2}\mathsf{F}_s, |\mathsf{F}_s|^{-1/2}\mathsf{F}_s\mathsf{T}_{cs}|\mathsf{T}_{cs}^T||\mathsf{F}_s|, \mathsf{F}_s\mathsf{T}_{cs}|\mathsf{T}_{cs}^T|\Big\}, \tag{18}$$

where the last four correspond to $\alpha = 0,\ 1/2$ in Eq.(13), and $\alpha = 1/2$ and 1 in Eq.(14). In the last four splittings, only the matrix $\mathsf{T}_{cs}|\mathsf{T}_{cs}^T|$ has to be pre-computed and stored. This matrix is skew-symmetric with ± 1 in the non-zero off-diagonal elements. Then, the Gershgorin circle theorem can be applied

$$\rho(\mathsf{T}_{cs}|\mathsf{T}_{cs}^T|\mathsf{F}_s) \leq \max\{|\mathsf{T}_{cs}|\mathsf{T}_{cs}^T|||\,\mathrm{diag}(|\mathsf{F}_s|)\}, \tag{19}$$

$$\rho(\mathsf{F}_s\mathsf{T}_{cs}|\mathsf{T}_{cs}^T|) \leq \max\{\mathrm{diag}(|\mathsf{F}_s|) \circ |\mathsf{T}_{cs}|\mathsf{T}_{cs}^T|\mathbf{1}_s\}, \tag{20}$$

to find an upper bound of their eigenvalues, which, in this case, lie on the imaginary axis. However, in practical flows, none of these approaches is able to provide better (or, at least, similar estimates) as applying

the Gershgorin circle theorem directly to the matrix $\mathsf{C}_c(\boldsymbol{u}_s)$. A simple explanation for this is that matrix $|\mathsf{T}_{cs}|\mathsf{T}_{cs}^T||\mathsf{F}_s$ has more non-zero off-diagonal coefficients per row than the matrix $\mathsf{T}_{cs}^T\mathsf{F}_s|\mathsf{T}_{cs}|$, *e.g.* for a structured Cartesian mesh in d-dimensions, the former has $2(2d-1)$ whereas the latter has only $2d$ non-zeros. Hence, more mass fluxes (in absolute value) are contributing to the Gershgorin circle radii.

Theorem 2 (Perron–Frobenius theorem by Perron (1907); Frobenius (1912))**.** *Given a real positive square matrix, i.e.* $\mathsf{A} \in \mathbb{R}^{n\times n}$ *and* $[\mathsf{A}]_{ij} > 0 \ \forall i,j$ *, it has a unique largest (in magnitude) real eigenvalue,* $r \in \mathbb{R}^+$*, with a corresponding eigenvector,* $\boldsymbol{v} \in \mathbb{R}^n$*, with strictly positive components, i.e.*

$$A\boldsymbol{v} = r\boldsymbol{v} \Rightarrow |\lambda| < r \ \textit{and} \ \boldsymbol{v}_i > 0 \ \ \forall i \in \{1,\dots,n\}, \tag{21}$$

where λ *denotes any eigenvalue of* A *except* r*, and* r *is the so-called Perron–Frobenius eigenvalue.*

Theorem 3 (Wielandt's theorem; see Gradshteyn and Ryzhik (2007))**.** *Given a matrix* $\mathsf{A} \in \mathbb{R}^{n\times n}$ *that satisfies the conditions of the Perron–Frobenius theorem (see Theorem 2) and a matrix* $\mathsf{B} \in \mathbb{R}^{n\times n}$ *such as*

$$|b_{ij}| \le a_{ij} \qquad \forall i,j, \tag{22}$$

where $b_{ij} = [\mathsf{B}]_{ij}$ *and* $a_{ij} = [\mathsf{A}]_{ij}$*. Then, any eigenvalue* λ^{B} *of* B *satisfies the inequality* $|\lambda^{\mathsf{B}}| \le r$ *where* r *is the Perron–Frobenius eigenvalue of* A*.*

Theorem 4 (Lemma 2 in Nikiforov (2007))**.** *Let* $\mathsf{A} \in \mathbb{R}^{n\times n}$ *be an irreducible non-negative symmetric matrix and* $\mathsf{R} \in \mathbb{R}^{n\times n}$ *be the diagonal matrix of its rowsums,* $[\mathsf{R}]_{ii} = \sum_{j=1}^{n}[\mathsf{A}]_{ij}$*. Then*

$$\rho\left(\mathsf{R} + \frac{1}{q-1}\mathsf{A}\right) \ge \frac{q}{q-1}\rho(\mathsf{A}), \tag{23}$$

with equality holding iff all rowsums of A *are equal.*

To circumvent this problem with the bounds of the spectral radius of the convective term, $\mathsf{C}_c(\boldsymbol{u}_s)$, we can use the Wielandt's theorem (see Theorem 3) to relate the spectral radius of the matrices

$$2\mathsf{C}_c(\boldsymbol{u}_s) \equiv \mathsf{T}_{cs}^T\mathsf{F}_s|\mathsf{T}_{cs}| \ , \ \mathsf{D}_c^{\mathsf{C}} \equiv -\mathsf{T}_{cs}^T|\mathsf{F}_s|\mathsf{T}_{cs}, \tag{24}$$

where $\mathsf{C}_c(\boldsymbol{u}_s)$ is the same convective operator defined in Eq.(10) and $\mathsf{D}_c^{\mathsf{C}} \in \mathbb{R}^{n\times n}$ is a diffusive-like operator where the face diffusivities are replaced by the magnitude of the mass fluxes, $|\mathsf{F}_s|$. The matrix $\mathsf{C}_c(\boldsymbol{u}_s)$ is zero-diagonal whereas $\mathsf{D}_c^{\mathsf{C}}$ has strictly negative diagonal coefficients. It is worth noticing that the off-diagonal elements of $2\mathsf{C}_c(\boldsymbol{u}_s)$ (in absolute value) and $\mathsf{D}_c^{\mathsf{C}}$ are equal. Hence, the zero-diagonal matrix

$$\mathsf{D}_c^{\mathsf{C},\text{off}} \equiv \mathsf{D}_c^{\mathsf{C}} - \text{diag}(\text{diag}(\mathsf{D}_c^{\mathsf{C}})) = 2|\mathsf{C}_c(\boldsymbol{u}_s)|, \tag{25}$$

satisfies the conditions of the Perron–Frobenius theorem (see Theorem 2). Then, we can apply Wielandt's theorem (Theorem 3) since

$$2|[\mathsf{C}_c(\boldsymbol{u}_s)]_{ij}| \le [\mathsf{D}_c^{\mathsf{C},\text{off}}]_{ij} \Rightarrow 2|\lambda^{\mathsf{C}}| \le \rho(\mathsf{D}_c^{\mathsf{C},\text{off}}) \tag{26}$$

In our case, taking $\mathsf{R} = -\text{diag}(\text{diag}(\mathsf{D}_c^{\mathsf{C}}))$, $\mathsf{A} = \mathsf{D}_c^{\mathsf{C},\text{off}}$ and $q = 2$ in Eq.(23) of Theorem 4 together with the inequality (26) leads to

$$\begin{aligned}\rho(|\mathsf{D}_c^{\mathsf{C}}|) &\overset{\text{Thm 4}}{\ge} 2\rho(\mathsf{D}_c^{\mathsf{C},\text{off}}) \overset{(25)}{=} \\ 4\rho(|\mathsf{C}_c(\boldsymbol{u}_s)|) &\overset{(26)}{\ge} 4\rho(\mathsf{C}_c(\boldsymbol{u}_s)).\end{aligned} \tag{27}$$

Recalling that the *leitmotiv* for all this analysis was to avoid constructing the matrix $\mathsf{C}_c(\boldsymbol{u}_s)$, it is obvious that relying on the construction of another (similar in structure) matrix such as $|\mathsf{D}_c^{\mathsf{C}}|$ would not make much sense. At this point, we can make use of the following properties of incidence and adjacency matrices

$$|\mathsf{T}_{cs}^T\mathsf{T}_{cs}| = |\mathsf{T}_{cs}^T||\mathsf{T}_{cs}|, \tag{28}$$

$$\left|\mathsf{T}_{cs}^T|\mathsf{F}_s|\mathsf{T}_{cs}\right| = |\mathsf{T}_{cs}^T||\mathsf{F}_s||\mathsf{T}_{cs}|, \tag{29}$$

to show that

$$\begin{aligned}\rho(|\mathsf{D}_c^{\mathsf{C}}|) = \rho\left(\left|\mathsf{T}_{cs}^T|\mathsf{F}_s|\mathsf{T}_{cs}\right|\right) &\overset{(29)}{=} \rho(|\mathsf{T}_{cs}^T||\mathsf{F}_s||\mathsf{T}_{cs}|) \\ &\overset{\text{Thm 1}}{=} \rho(|\mathsf{T}_{cs}||\mathsf{T}_{cs}^T||\mathsf{F}_s|) \overset{(28)}{=} \rho(|\mathsf{T}_{cs}\mathsf{T}_{cs}^T||\mathsf{F}_s|).\end{aligned} \tag{30}$$

Then, recalling the inequality (27), we can finally show that $\rho(\mathsf{C}_c(\boldsymbol{u}_s))$ can be bounded with $\rho(|\mathsf{F}_s|^{\alpha}|\mathsf{T}_{cs}\mathsf{T}_{cs}^T||\mathsf{F}_s|^{1-\alpha})$, *i.e.*

$$\begin{aligned}\rho(|\mathsf{F}_s|^{\alpha}|\mathsf{T}_{cs}\mathsf{T}_{cs}^T||\mathsf{F}_s|^{1-\alpha}) &\overset{\text{Thm 1}}{=} \rho(|\mathsf{T}_{cs}\mathsf{T}_{cs}^T||\mathsf{F}_s|) \\ &\overset{(30)}{=} \rho(|\mathsf{D}_c^{\mathsf{C}}|) \overset{(27)}{\ge} 4\rho(\mathsf{C}_c(\boldsymbol{u}_s)),\end{aligned} \tag{31}$$

regardless of the value of α.

Remark 2. *In case the discrete convective term is not skew-symmetric, the method can be easily adapted as follows: imaginary contributions still come from* $\mathsf{C}_c(\boldsymbol{u}_s)$ *whereas negative real-valued contributions are added to the diffusive term by replacing*

$$\tilde{\Lambda}_s \longrightarrow \tilde{\Lambda}_s + \frac{1}{2}\,\text{diag}(|\mathsf{F}_s|(\mathbf{1}_s - \boldsymbol{\Psi}_s)) \tag{32}$$

where $\boldsymbol{\Psi}_s \in \mathbb{R}^m$ *is a vector that defines the local blending factor between symmetry-preserving (*$\Psi = 1$*) and upwind schemes (*$\Psi = 0$*).*

5 Numerical tests

Shortly, the newly proposed *AlgEigCD* method simply relies on the construction of the matrix $|\mathsf{T}_{cs}\Omega_c^{-1}\mathsf{T}_{cs}^T|$ which can be done at the pre-processing stage. Then, this matrix is used to compute eigenbounds of matrices $\Omega_c^{-1}\mathsf{D}$ and $\Omega_c^{-1}\mathsf{C}(\boldsymbol{u}_s)$ as follows

$$\begin{aligned}\rho(\Omega_c^{-1}\mathsf{C}_c(\boldsymbol{u}_s)) &\le 1/4\rho(|\mathsf{T}_{cs}\Omega_c^{-1}\mathsf{T}_{cs}^T||\mathsf{F}_s|) \\ &\le 1/4\max\{|\mathsf{T}_{cs}\Omega_c^{-1}\mathsf{T}_{cs}^T|\,\text{diag}(|\mathsf{F}_s|)\},\end{aligned} \tag{33}$$

$$\begin{aligned}\rho(\Omega_c^{-1}\mathsf{D}_c(\boldsymbol{\alpha}_s)) &= \rho(\ \mathsf{T}_{cs}\Omega_c^{-1}\mathsf{T}_{cs}^T\ \tilde{\Lambda}_s\ ) \\ &\le \max\{|\mathsf{T}_{cs}\Omega_c^{-1}\mathsf{T}_{cs}^T|\,\text{diag}(\ \tilde{\Lambda}_s\ )\},\end{aligned} \tag{34}$$

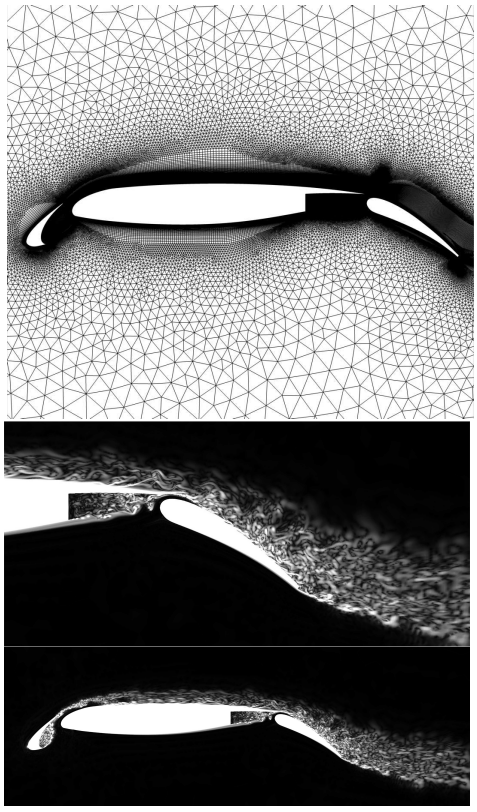

Figure 3: 30P30N multi-element high-lift airfoil. Top: zoom around the airfoil of the unstructured mesh used. Bottom: visualization of the vorticity magnitude at $Re = 10^6$ and an angle of attack of 5.5^o.

where the former inequality follows from Eq.(31) and the application of the Gershgorin circle theorem to matrix $|\mathsf{T}_{cs}\mathsf{T}_{cs}^T||\mathsf{F}_s|$. Similarly, for the latter and Eq.(16). Notice that in these cases, the diagonal matrix Ω_c^{-1} has been introduced (see Remark 1). Also notice that among all the possible values we have chosen $\alpha = 0$ since it consistently provided the best estimations for different test-cases (not shown here) for both structured and unstructured meshes.

The performance of this methodology is tested and compared with a classical CFL criterion given by

$$\Delta t_{CFL} = \min\left\{\frac{C_C}{\lambda^{\mathsf{C}}_{CFL}}, \frac{C_D}{\lambda^{\mathsf{D}}_{CFL}}\right\} \quad \text{where} \qquad (35)$$

$$\lambda^{\mathsf{C}}_{CFL} = \max_f\left\{\frac{[\boldsymbol{u}_s]_f}{\delta_f}\right\}, \lambda^{\mathsf{D}}_{CFL} = \max_f\left\{\frac{4\nu_f}{d\delta_f^2}\right\},$$

where d is the number of spatial directions and the values of C_C and C_D are set to 0.35 and 0.8, respectively. These values were used in combination with an AB2 scheme in the first versions of our in-house STG code to guarantee that all the eigenvalues lie inside the stability region regardless of the flow conditions.

The tested configuration corresponds to a 3D flow around a 30P30N multi-element high-lift airfoil at an angle of attack of 5.5^o (see Figure 3). The mesh is unstructured with $\approx 12.5M$ control volumes combining hexahedral elements ($\approx 8.2M$) and triangular prisms ($\approx 4.3M$). Flow fields have been obtained with the in-house NOISEtte code by Gorobets and Bakhvalov (2022). Results for a wide range of Re are shown in Figure 4 (left). As expected for low-Re, the diffusive term is dominant, *i.e.* $\varphi \approx 0$ whereas for (very) high-Re the convective term becomes the dominant one. Regarding the ratio $\langle \Delta t_{AlgEigCD+\kappa 1L2}\rangle \,/\, \langle \Delta t_{CFL+AB2}\rangle$ in this case it takes values around 4 for $Re \lesssim 10^6$ and goes down to approximately 2 at $Re = 10^7$. Notice that for the range of Re-numbers, this mesh is designed for (see Figure 3, right), the overall gain in terms of Δt is approximately 4. This overall gain results from a combination of factors, which are analyzed in detail in Figure 4 (right) where the ratio $\langle \Delta t_{AlgEigCD+\kappa 1L2}\rangle$ is compared with the $\langle \Delta t\rangle$ obtained with other three approaches apart from the $CFL + AB2$. Namely, (i) *EigenCD*+$\kappa 1L2$ is the same as *AlgEigCD*+$\kappa 1L2$ but directly using the Gershgorin circle theorem to matrices $\Omega_c^{-1}\mathsf{C}_c\,(\boldsymbol{u}_s)$ and $\Omega_c^{-1}\mathsf{D}_c$. Interestingly enough, the new method provides slightly better estimations. Nevertheless, the main advantage respect to the $EigenCD$ method proposed in Trias and O. Lehmkuhl (2011) is that the new method does not require to compute the coefficients of the matrix and it relies on very simple algebraic kernels, which simplifies its implementation and guarantees cross-platform portability. Then, (ii) $AlgEigCD + \kappa 1L2$ with $\kappa = 1/2$ consists on using the new $AlgEigCD$ method to compute the eigenbounds of the convective and diffusive operators but forcing $\kappa = 1/2$. Finally, the approach (iii) *AlgEigCD*+AB2 is basically the same as the $CFL + AB2$ method given in Eq.(35) but replacing $\lambda^{\mathsf{C}}_{CFL}$ and $\lambda^{\mathsf{D}}_{CFL}$ by the values obtained with the new *AlgEigCD* method. Therefore, in this case, the differences respect to $\langle \Delta t_{AlgEigCD+\kappa 1L2}\rangle$ are due to the self-adaptivity of the $\kappa 1L2$ scheme. Therefore, the difference between this last method and the $CFL + AB2$ method can only be attributed to the inaccuracy in the computation of $\lambda^{\mathsf{C}}_{CFL}$ and $\lambda^{\mathsf{D}}_{CFL}$ in Eq.(35). From the results shown in Figure 4, it becomes clear that the expression used to compute $\lambda^{\mathsf{D}}_{CFL}$ is quite inaccurate for unstructured grids.

6 Concluding remarks

Numerical results of the new *AlgEigCD* method have shown a significant gain respect to a classical CFL condition, especially for unstructured meshes, leading to CPU cost reductions up to approximately 4. This observation was already done in Trias and O. Lehmkuhl (2011) where the *EigenCD* method was proposed. Nevertheless, the new method is slightly improving the former one. However, the key elements of the newly proposed *AlgEigCD* are the fact that no new matrix have to be re-computed every time-step and that, in practice, only relies on a sparse matrix-vector product where only the vectors $\mathrm{diag}(|\mathsf{F}_s|)$ and

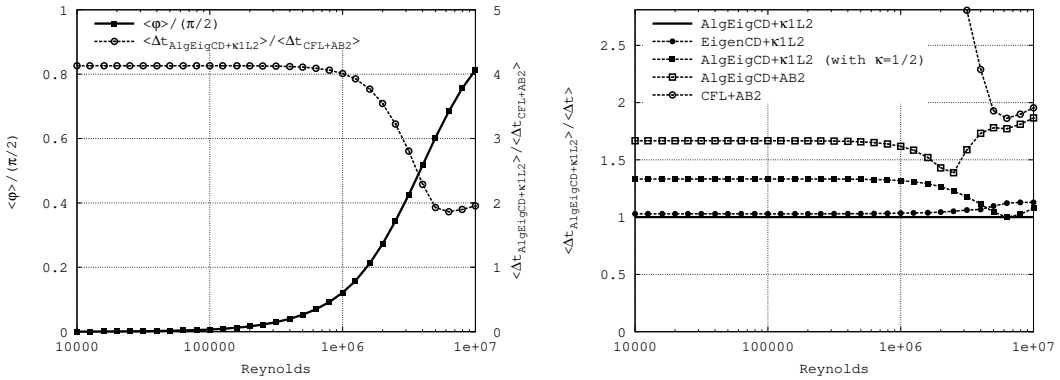

Figure 4: Numerical results obtained for the high-lift airfoil 30P30N displayed in Figure 3 at different Reynolds numbers using the same mesh. Left: average $\varphi = \tan^{-1}(|\lambda^{\mathsf{C}}_{\max}|/|\lambda^{\mathsf{D}}_{\max}|)$ and ratio between the time-step $\Delta t^{AlgEigCD+\kappa 1L2}$, computed using the *AlgEigCD* method in conjunction with the self-adaptive $\kappa 1L2$ time-integration method, and $\Delta t^{CFL+AB2}$ obtained with the more classical CFL condition given in Eq.(35). Right: comparison of $\langle \Delta t_{AlgEigCD+\kappa 1L2} \rangle$ with the $\langle \Delta t \rangle$ obtained with other three approaches apart from the $CFL + AB2$.

$\mathrm{diag}(\tilde{\Lambda}_s)$ change on time. Hence, implementation and cross-platform portability are straightforward.

Although the proposed methodology has been deduced in the context of the symmetry-preserving spatial discretization, it can be easily applied to other schemes resulting from some sort of blending, *e.g.* hybrid schemes, flux limiters, etc, between the symmetry-preserving and the first-order upwind scheme (see Remark 2). Finally, it worth mentioning that we have plans to extend this method to other time-integration schemes with larger stability domains and subsequently larger time-steps.

Acknowledgments

F.X.T., J.A.H, D.S and A.O. are supported by the *Ministerio de Economía y Competitividad*, Spain, RETOtwin project (PDC2021-120970-I00). Calculations were carried out on MareNostrum 4 supercomputer at BSC. We thankfully acknowledge these institutions.

References

Dabbagh, F., Trias, F. X., Gorobets, A., and Oliva, A. (2020). Flow topology dynamics in a three-dimensional phase space for turbulent Rayleigh-Bénard convection. *Physical Review Fluids*, 5:024603.

Felten, F. N. and Lund, T. S. (2006). Kinetic energy conservation issues associated with the collocated mesh scheme for incompressible flow. *Journal of Computational Physics*, 215:465–484.

Frobenius, G. (1912). Ueber Matrizen aus nicht negativen Elementen. *Sitzungsberichte der Königlich Preussischen Akademie der Wissenschaften*, page 456477.

Gorobets, A. and Bakhvalov, P. (2022). Heterogeneous cpu+gpu parallelization for high-accuracy scale-resolving simulations of compressible turbulent flows on hybrid supercomputers. *Computer Physics Communications*, 271:108231.

Gradshteyn, S. I. and Ryzhik, I. M. (2007). *Tables of Integrals, Series, and Products*. Elsevier, Academic Press, 7th edition.

Hopman, J. A., Alsalti-Baldellou, A., Trias, F. X., and Oliva, A. (2023). On a conservative solution to checkerboarding: examining the causes of non-physical pressure modes. In *14^{th} International ERCOFTAC symposium on engineering, turbulence, modelling and measurements (ETMM14)*, Barcelona.

Komen, E., Hopman, J. A., Frederix, E. M. A., Trias, F. X., and Verstappen, R. W. C. P. (2021). A symmetry-preserving second-order time-accurate PISO-based method. *Computers & Fluids*, 225:104979.

Komen, E. M. J., Camilo, L. H., Shams, A., Geurts, B. J., and Koren, B. (2017). A quantification method for numerical dissipation in quasi-DNS and under-resolved DNS, and effects of numerical dissipation in quasi-DNS and under-resolved DNS of turbulent channel flows. *Journal of Computational Physics*, 345:565–595.

Nikiforov, V. (2007). Chromatic number and spectral radius. *Linear Algebra and its Applications*, 426:810–814.

Perron, O. (1907). Zur Theorie der Matrices. *Mathematische Annalen*, 64:248–263.

Santos, D., Trias, F. X., and Verstappen, R. W. C. P. (2023). An energy-preserving unconditionally stable fractional step method with high order operators on collocated unstructured grids. In *14^{th} International ERCOFTAC symposium on engineering, turbulence, modelling and measurements (ETMM14)*, Barcelona.

Trias, F. X., Gorobets, A., and Oliva, A. (2015). Turbulent flow around a square cylinder at Reynolds number 22000: a DNS study. *Computers & Fluids*, 123:87–98.

Trias, F. X. and O. Lehmkuhl (2011). A self-adaptive strategy for the time-integration of Navier-Stokes equations. *Numerical Heat Transfer, part B*, 60(2):116–134.

Trias, F. X., O. Lehmkuhl, A. Oliva, C.D. Pérez-Segarra, and R.W.C.P. Verstappen (2014). Symmetry-preserving discretization of Navier-Stokes equations on collocated unstructured meshes. *Journal of Computational Physics*, 258:246–267.

Verstappen, R. W. C. P. and Veldman, A. E. P. (2003). Symmetry-Preserving Discretization of Turbulent Flow. *Journal of Computational Physics*, 187:343–368.